Supporting Information for "Tertiary Plasticity Drives the Efficiency of Enterocin 7B Interactions With Lipid Membranes"

Yi Zhuang,[†] Stephen Quirk,[‡] Erica R. Stover,[†] Hailey R. Bureau,[†] Caley R. Allen,[†] and Rigoberto Hernandez[*,†,¶,§]

[†]*Department of Chemistry, Johns Hopkins University, Baltimore, MD 21218, USA*

[‡]*Kimberly-Clark Corporation, Atlanta, GA 30076-2199*

[¶]*Department of Chemical & Biomolecular Engineering, Johns Hopkins University, Baltimore, MD 21218, USA*

[§]*Department of Materials Science & Engineering, Johns Hopkins University, Baltimore, MD 21218, USA*

E-mail: r.hernandez@jhu.edu

Introduction

In this supporting document, we provide additional detail in support of our conclusion that tertiary plasticity is critical in providing the effects found in 2M60 as summarized in the main text. Specifically, we demonstrate that the protein function is lost if we lock its core. We report the structural properties of the WT 2M60 and the mutants in more detail than available in the main document. A pair-wise comparison of the potential of mean force (PMF) of unfolding under 10 Å/ns pulling speed provides evidence that the relative trends between the mutants hold true for different pulling speeds. In addition, we also report an analysis on the change in hydrogen bonds for each helical region of each peptide.

On the tertiary plasticity of 2M60 and its mutants

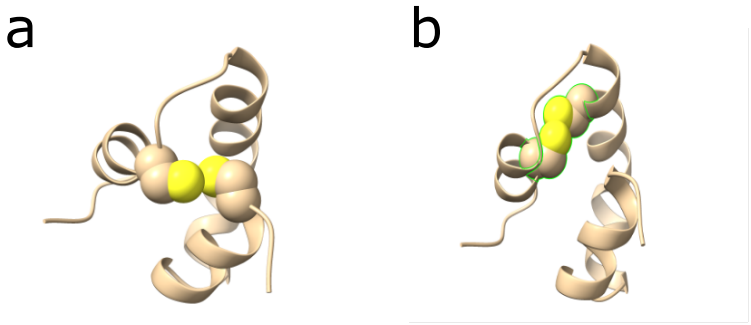

Figure S1: Three dimensional model of the core-locked disulfide enterocin mutants. A) Ala3Cys-Ile33Cys (3-33). B) Phe26Cys-Ile36Cys (26-36).

The original hypothesis for the work presented in this paper was that leaderless enterocin antimicrobial peptides function more efficiently if the interactions in the hydrophobic core were more plastic; that is more easily disrupted. To initially investigate this hypothesis, two 'core-locked' mutations were designed and tested. The first mutation consisted of an engineered disulfide bond between residues Phe26 and Ile36 (termed 26-36), which locked helices 2 and 3 together. The second introduced disulfide was between residues Ala3 and Ile33 (termed 3-33), locking helices 1 and 3 together. Both disulfides incorporated the most

probable cysteine rotomers (as determined by the ROTOMER tool in ChimeraX) and are both within allowed Ramachandran space. The sulfur-sulfur bond distances for the two mutants are 3.1 Å (3-33) and 2.7 Å (26-36). The model structures of the two mutants are shown in Fig. S1.

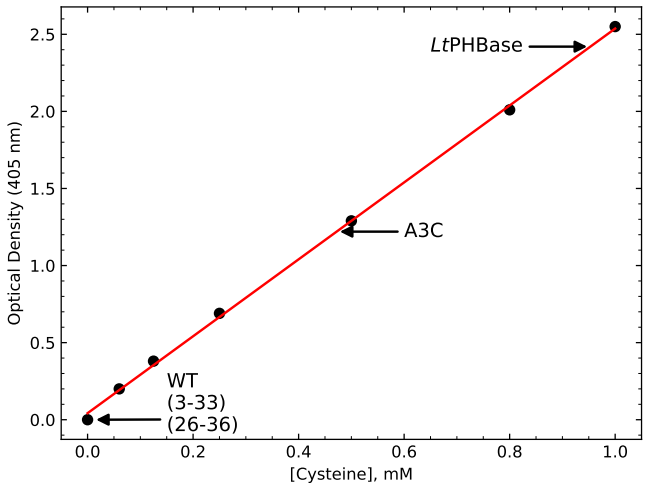

Figure S2: DTNB assay. Free cysteine (between 0 and 1 mM) was reacted with Ellman's reagent and the optical density at 405 nm was recorded to create a standard curve of optical density versus the cysteine concentration. Enterocin peptides at a concentration of 0.5 mM were reacted with DNTB- WT, (3-33), and (26-36). Their optical density readings are noted on the standard curve, as is a single cysteine containing enterocin mutant (A3C) and a control protein that contains two free cysteine residues (both also at 0.5 mM).

To ensure that the disulfide bond was formed in both peptides, a free sulfhydryl assay was undertaken using the DTNB Thiol Assay kit from Ethos Bioscience (Logan Township, NJ). Fig. S2 indicates that there is no cysteine reactivity with either (3-33) or (26-36), indicating that the disulfide is formed in both mutants. A control peptide that contained on cysteine, Ala3Cys, gave the expected 405 nm optical density relative to the free cysteine standard curve, as did a protein (*Lt*PHBase) that contained two free cysteines.

Far and Near UV CD spectroscopy were undertaken to ensure that both core-locked mutants were properly folded. Both mutants retain nearly identical secondary (Far UV) and tertiary (Near UV) structure as the wild-type peptide, as shown in Fig. S3. This indicates

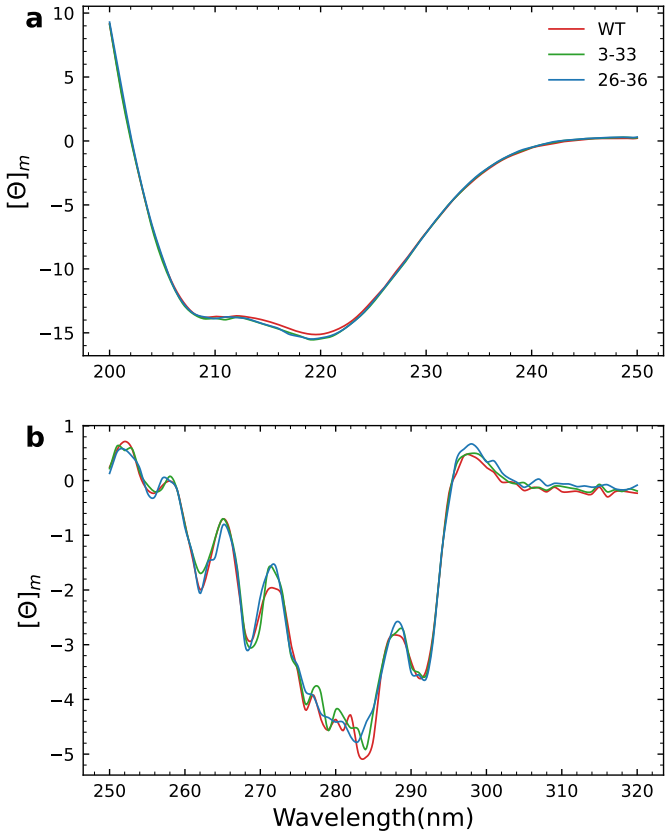

Figure S3: Secondary and tertiary structure of the two core-locked disulfide enterocin mutants. A) Far UV CD spectra plotted as the mean molar ellipticity versus wavelength at 10 μM peptide. B) Near UV CD spectra plotted as the mean molar ellipticity versus wavelength at 50 μM peptide. Lines represent the average of two independent determinations.

that the introduced disulfide bond does not disrupt native structure.

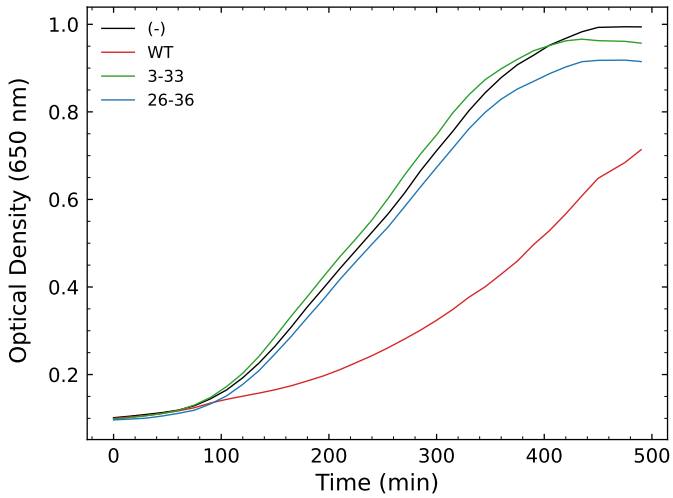

Figure S4: Growth curve of *Bacillus subtilis* in the presence of 50 μM of either core-locked peptide, 2 μM of wild-type enterocin 7B, or no added peptide. Peptide was added a time = 0 minutes and growth was continued for 450 minutes at 37 °C. Lines represent the average of three independent determinations.

When either core-locked peptide is added (at concentrations between 10 and 100 μM) to a newly inoculated culture of *Bacillus subtilis*, the bacterial culture can display growth kinetics nearly identical to the no-peptide control. Fig. S4 illustrates the growth curves for 50 μM of either core-locked peptide compared to 2 μM of wild-type enterocin. The lack of killing ability of the core-locked mutants made it impossible to calculate a meaningful MIC. Essentially although retaining wild-type topology, both core-locked mutants are unable to kill *B. subtilis*.

This lack of function in the two core-locked mutants extended to the interaction between the core-locked mutants and synthetic PG:PE unilamellar liposomes. Neither core-locked mutant was capable of disrupting the liposomes as shown in Fig. S5; as evidenced by the lack of released calcein over the course of the assay compared to the wild-type peptide. Both activity measures indicate that an enterocin 7B peptide that is unable to unfold its hydrophobic core is incapable of initiating membrane disruption that leads to bacterial lysis and death. Although the core-locked mutants cannot be unfolded or pulled in a ASMD

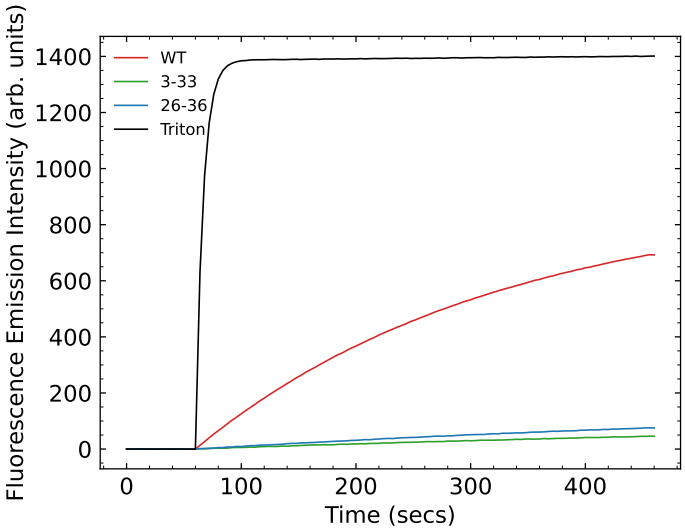

Figure S5: Release kinetics of calcein from 1:1 PG:PE liposomes (200 μM). At t = 60 seconds either wild-type peptide at 10 μM, 50 μM disulfide mutant peptide, or Triton X-100 (final concentration of 10% w/v) was added to each well and calcein release was measured with an excitation wavelength of 500 nm and an emission wavelength of 520 nm.

computation due to the presence of a covalent bond between adjacent helices, they served to preliminarily confirm the hypothesis that tertiary plasticity drives enterocin 7B interactions with bacterial membranes. It led to the identification of seven arginine scanning mutations that differentially destabilized enterocin 7B hydrophobic core.

Supporting Materials

The optical density as a function of Enterocin mutant concentration is analyzed in Fig. S6. In addition, the structural analysis gained from VMD[1] and ChimeraX[2] is shown in Table. S1 and Table. S2. All mutants have similar volume sizes to the WT; however, the solvent accessible surface area (SASA) and R_g values of mutants are all higher than WT. Furthermore, the root mean-square deviation (RMSD) values of the prepared mutants range from 1.48 Å to 4.12 Å.

During the adaptive steered molecular dynamics (ASMD) simulations, all peptides were compressed to 15 Å end-to-end distance initially so that they could sample structures smaller

and larger than those with local minimum energies. The respective comparison of the PMF between WT and each mutant is shown in Fig. S9 with error analysis accumulatively calculated over stages based on Eq. S1[3]

$$\delta E_{\mathrm{acc}}(t) = \sqrt{\sum_{i=1}^{S-1} \delta E_i(t_i)^2 + \delta E_S(\delta t)^2;}, \tag{S1}$$

where δE_i represents the error for stage i, and each t_i is the time at the end of stage i. In addition, as the WT is composed of three helical regions, the hydrogen bond profile for each helical region was recorded and shown in Fig. S12. The fraction of native contact over the stretch was also calculated through MDTraj[4] based on Ref. 5 with β as 50/nm, λ as 1.8 and native cutoff as 0.45 nm for all peptides. The result was shown in Fig. S13, which is determined via Eq. 5 in the main text.

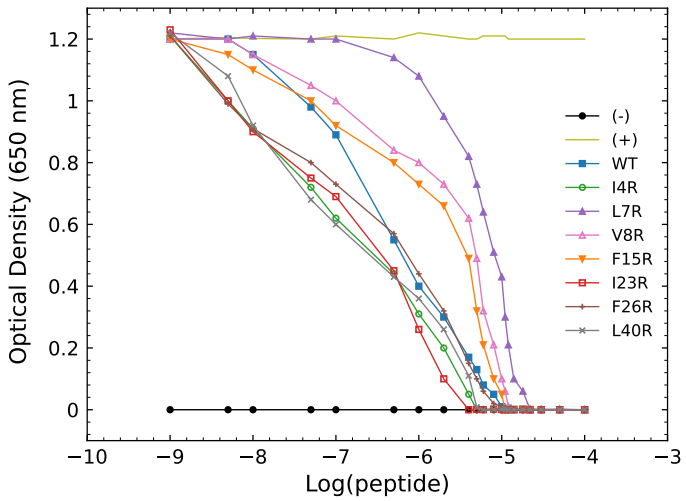

Figure S6: The optical density as a function of Enterocin mutant concentration, including WT (closed squares), I4R (open circles), L7R (closed triangles), V8R (open triangles), F15R (closed inverted triangles), I23R (open squares), F26R (pluses), L40R (crosses), the cell density control (solid curve), and the sterility control (closed circle).

Table S1: Structural properties of Enterocin peptide structures

Peptide	Vol. (Å^3)	SASA (Å^3)	R_g (Å)	RMSD (Å)
WT	6,111	3,423	9.79	0.0
I4R	6,099	3,588	10.11	2.87
L7R	6,032	3,849	10.40	3.27
V8R	6,126	3,511	9.84	1.53
F15R	6,020	3,485	9.91	1.73
I23R	6,023	3,847	10.77	3.46
F26R	6,073	3,635	10.01	1.83
L40R	5,942	3,970	10.64	2.59

Table S2: RMSD (Å) between Enterocin peptides

Peptide	WT	I4R	L7R	V8R	F15R	I23R	F26R	L40R
WT	-	2.87	3.27	1.53	1.73	3.46	1.83	2.59
I4R		-	3.23	2.71	2.86	3.35	3.37	2.53
L7R			-	3.5	3.0	4.12	4.12	3.24
V8R				-	1.48	3.59	2.1	2.62
F15R					-	3.4	2.71	2.72
I23R						-	3.95	3.11
F26R							-	2.69
L40R								-

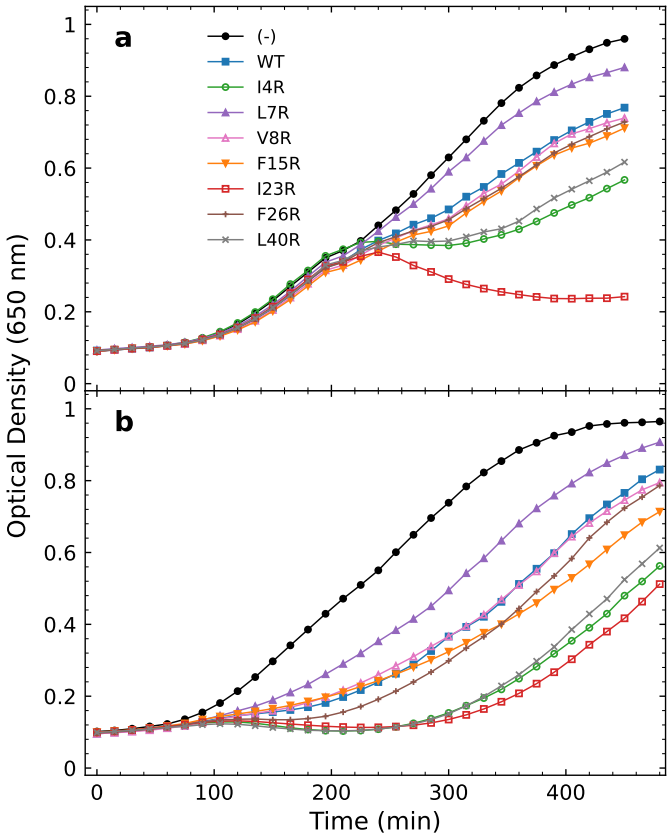

Figure S7: a) Growth curve of *Bacillus subtilis* in the presence of a sub-MIC level of Enterocin peptide. At time = 200 minutes, Enterocin peptides were added to the growing culture at a final concentration of two micromolar. Growth at 37 °C was continued for an additional 250 minutes. b) Growth curve of *Bacillus subtilis* in the presence of a sub-MIC level of Enterocin peptide. At time = 0 minutes, Enterocin peptides were added to a starting culture at a final concentration of two micromolar. Growth at 37 °C was initiated for a total of 450 minutes. Lines correspond to the average of three experiments. In both panels a and b, lines and symbols correspond to the average of three experiments for WT (closed squares), control with no peptide (closed circles), I4R (open circles), L7R (closed triangles), V8R (open triangles), F15R (closed inverted triangles), I23R (open squares), F26R (pluses) and L40R (crosses).

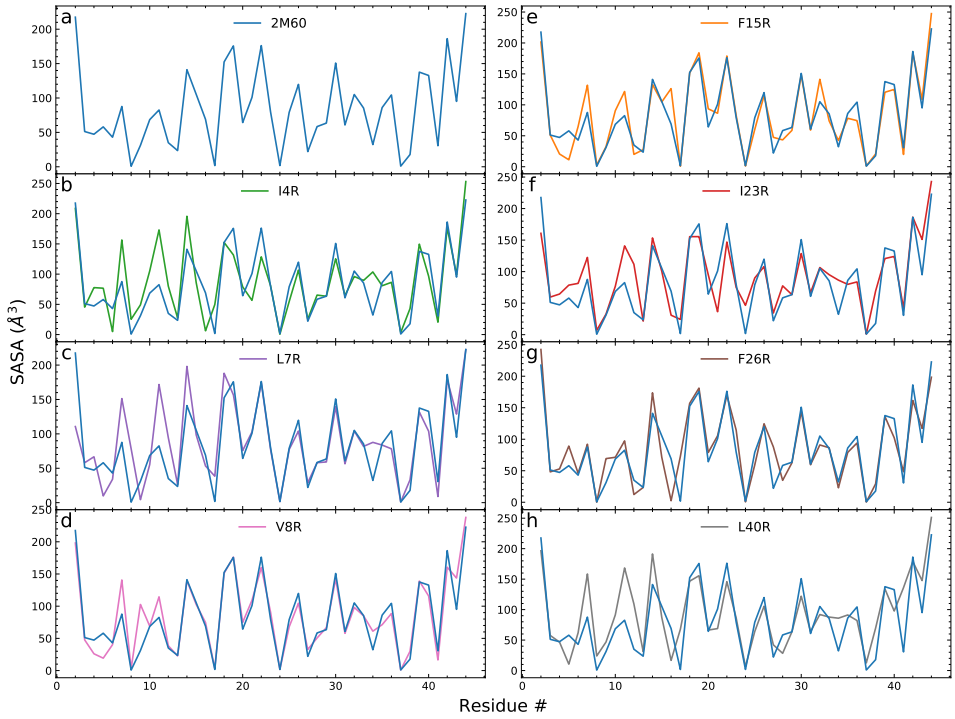

Figure S8: The average SASA around each residue over 100 equilibrated structures for each peptide as labeled in the legend. The probe radius was set as 1.4 Å.

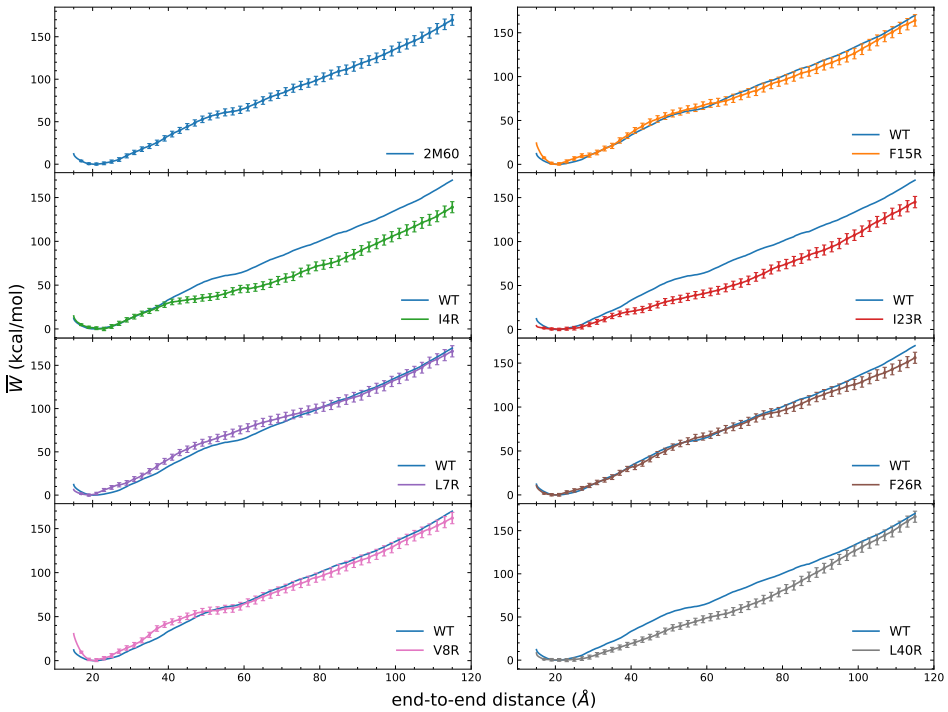

Figure S9: Comparison of the energetics of the wild type Enterocin 7B and each mutant with their cumulative errors. The PMF have been obtained using 100 trajectories per stage (tps) at 10 Å/ns.

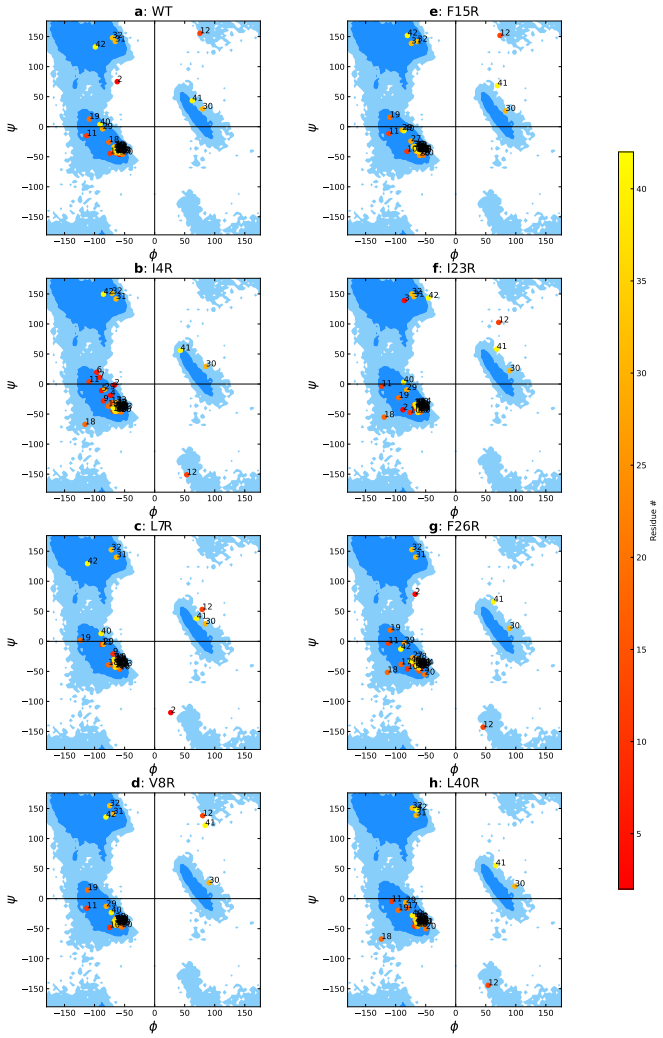

Figure S10: The Ramachandran plot for the equilibrated structures for WT 2M60 (a), and the seven mutants considered here: I4R (b), L7R (c), V8R (d), F15R (e), I23R (f), F26R (g) and L40R (h). Each point represents the average of the angles associated with a given residue over 100 equilibrated structures. The plots are generated using the MDAnalysis package,[6,7] and overlayed over contours for "allowed regions" (dark blue) and "marginally allowed" regions (light blue) as provided in the package.

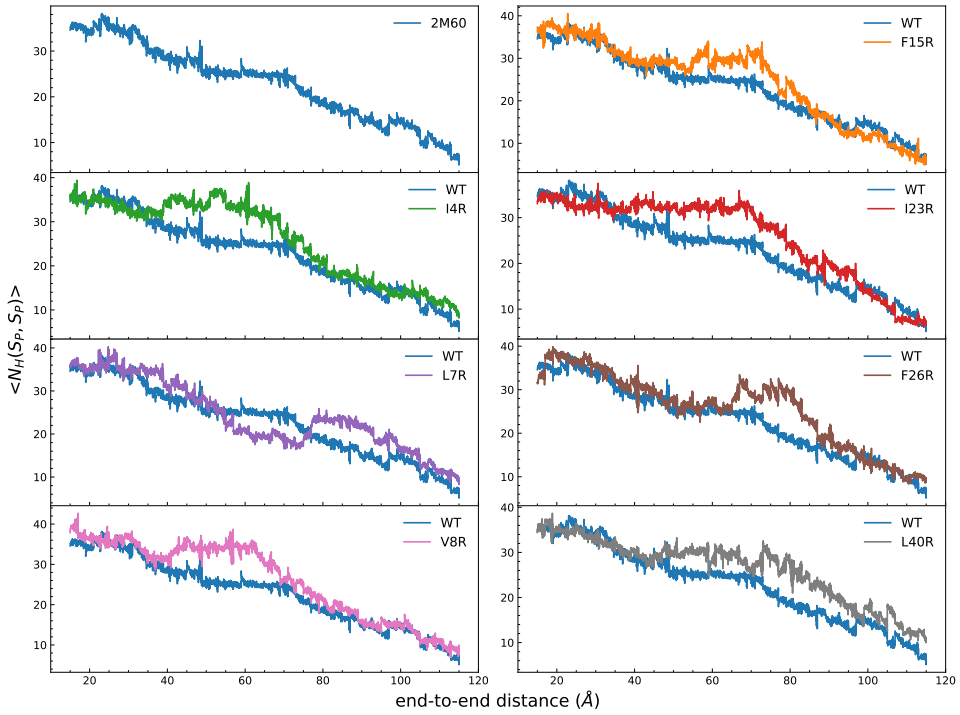

Figure S11: Comparison of intra-peptide hydrogen bond profiles between the wild type (WT) Enterocin 7B and each mutant along the stretching process in terms of relative ranking across the experimental and computational figures of merit reported here.

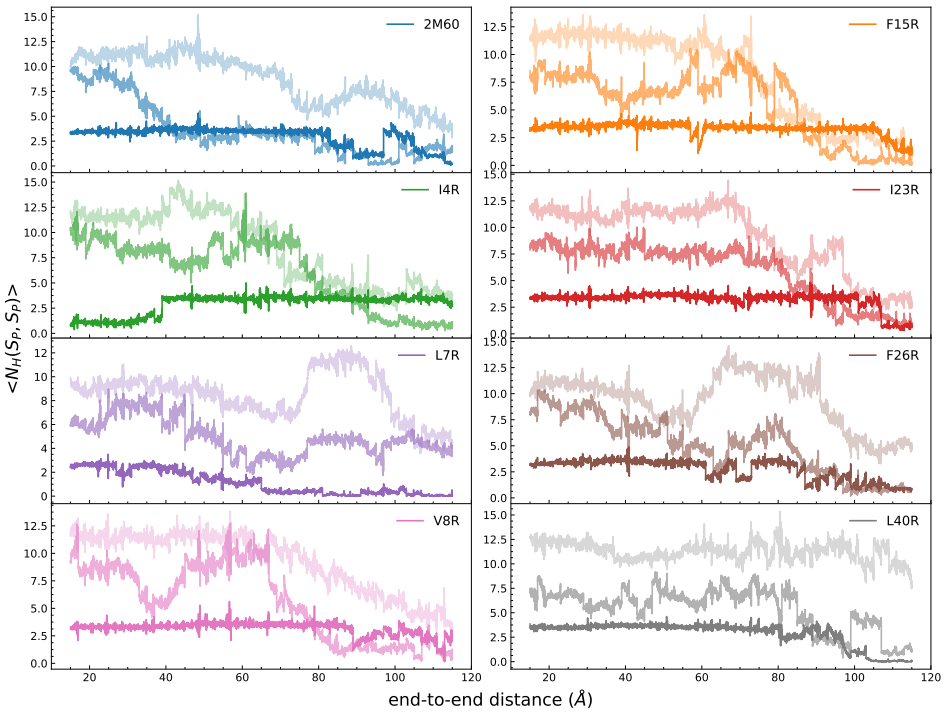

Figure S12: The comparison of the intra-peptide hydrogen bond for each helical region between the wild type Enterocin 7B and each mutant along the stretching process. Each helical region was rendered as different degrees of transparency from N-terminus as 0%, C-terminus (stretch end) as 40%, and middle region as 70%.

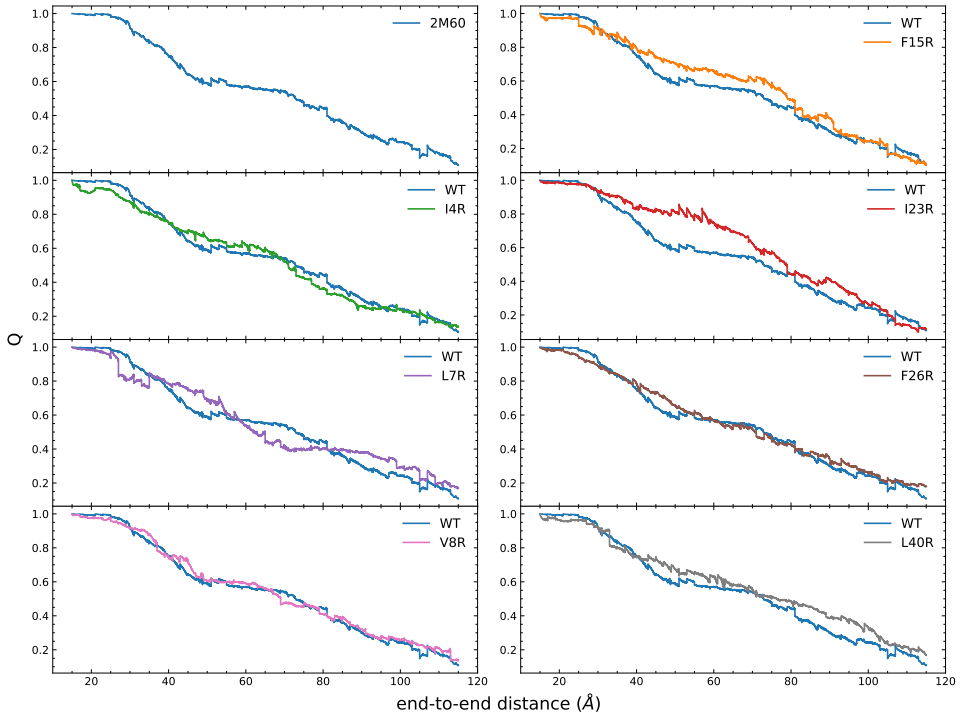

Figure S13: Comparison of the weighted average fraction of native contacts for each peptide over 100 tps. The fraction of native contacts for each trajectory was calculated through MDTraj[4] and then averaged over each stage using Eq. 5 in the main text.

References

(1) Humphrey, W.; Dalke, A.; Schulten, K. VMD - Visual Molecular Dynamics. *J. Molec. Graphics* **1996**, *14*, 33–38.

(2) Pettersen, E. F.; Goddard, T. D.; Huang, C. C.; Meng, E. C.; Couch, G. S.; Croll, T. I.; Morris, J. H.; Ferrin, T. E. UCSF ChimeraX: Structure visualization for researchers, educators, and developers. *Protein Sci.* **2021**, *30*, 70–82.

(3) Zhuang, Y.; Bureau, H.; Quirk, S.; Hernandez, R. Adaptive Steered Molecular Dynamics of Biomolecules. *Mol. Sim.* **2021**, *47*, 408–419.

(4) McGibbon, R. T.; Beauchamp, K. A.; Harrigan, M. P.; Klein, C.; Swails, J. M.; Hernandez, C. X.; Schwantes, C. R.; Wang, L.; Lane, T. J.; Pande, V. S. MDtraj: A Modern Open Library for the Analysis of Molecular Dynamics Trajectories. *Biophys. J.* **2015**, *109*, 1528–1532.

(5) Best, R. B.; Hummer, G.; Eaton, W. A. Native Contacts Determine Protein Folding Mechanisms in Atomistic Simulations. *Proc. Natl. Acad. Sci. U.S.A.* **2013**, *110*, 17874–17879.

(6) Michaud-Agrawal, N.; Denning, E. J.; Woolf, T. B.; Beckstein, O. MDAnalysis: A Toolkit for the Analysis of Molecular Dynamics Simulations. *J. Comput. Chem.* **2011**, *32*, 2319–2327.

(7) Gowers, R.; Linke, M.; Barnoud, J.; Reddy, T.; Melo, M.; Seyler, S.; Domański, J.; Dotson, D.; Buchoux, S.; Kenney, I. et al. In *Proceedings of the Python in Science Conference*; Benthall, S., Rostrup, S., Eds.; SciPy, 2016; pp 98–105.